Physics of the Earth and Planetary Interiors 261 (2016) 118–123

Contents lists available at ScienceDirect

Physics of the Earth and Planetary Interiors

journal homepage: www.elsevier.com/locate/pepi

Earthquake friction

Francesco Mulargia [a], Andrea Bizzarri [b,*]

[a] Dipartimento di Fisica e Astronomia, Università di Bologna, viale Berti Pichat 8, 40127 Bologna, Italy
[b] Istituto Nazionale di Geofisica e Vulcanologia, Sezione di Bologna, via Donato Creti 12, 40128 Bologna, Italy

ARTICLE INFO

Article history:
Received 12 January 2016
Received in revised form 26 May 2016
Accepted 8 June 2016
Available online 15 June 2016

Keywords:
Earthquake physics
Energy balance
Friction
Fluids
Thermal effects

ABSTRACT

Laboratory friction slip experiments on rocks provide firm evidence that the static friction coefficient μ has values ~0.7. This would imply large amounts of heat produced by seismically active faults, but no heat flow anomaly is observed, and mineralogic evidence of frictional heating is virtually absent. This stands for lower μ values ~0.2, as also required by the observed orientation of faults with respect to the maximum compressive stress. We show that accounting for the thermal and mechanical energy balance of the system removes this inconsistence, implying a multi-stage strain release process. The first stage consists of a small and slow aseismic slip at high friction on pre-existent stress concentrators within the fault volume but angled with the main fault as Riedel cracks. This introduces a second stage dominated by frictional temperature increase inducing local pressurization of pore fluids around the slip patches, which is in turn followed by a third stage in which thermal diffusion extends the frictionally heated zones making them coalesce into a connected pressurized region oriented as the fault plane. Then, the system enters a state of equivalent low static friction in which it can undergo the fast elastic radiation slip prescribed by dislocation earthquake models.

1. Introduction

Geological, physical and seismological evidence concur in establishing that frictional sliding of crustal masses is at the basis of earthquake dynamics.

Hence, as a fundamental equation of the fault slip process it can be taken the Tresca–Von Mises criterion (see e.g., Terzaghi et al., 1996), which prescribes that failure occurs when the effective stress σ^{eff} is larger than the "rupture" stress σ^{R}

$$\sigma^{eff} > \sigma^{R} \tag{1}$$

with

$$\sigma^{eff} = \sigma_S + \mu(\sigma_N - p_{fluid}) \tag{2}$$

where σ_S and σ_N are respectively the shear and normal stresses on the slip plane, μ is the (static) coefficient of friction and p_{fluid} the pore fluid pressure.

It should be emphasized that the slip failure process occurring in nature is considerably more complex than in both the classic and the most modern laboratory experiments (e.g., Sone and Shimamoto, 2009). First of all, even if there are some recent attempts to simulate gouge by using powdered materials (see Section 2 of Niemeijer et al., 2012 and references therein), the slip in laboratory experiments usually occurs on machined surfaces. Moreover, the confining pressure is comparatively modest, since the friction machines work at most at a few tens of MPa pressures, which is one order of magnitude less than the lithostatic ~10^2 MPa level of crustal hypocentral depths. Furthermore, the velocity attainable in laboratory experiments is limited to a few m/s (e.g., Sone and Shimamoto, 2009; Di Toro et al., 2010), which is also one order of magnitude lower than fault slip velocities of real world events (Ohnaka, 2013). In addition, the fault zone boundaries in the laboratory configurations are necessarily planar, smooth and small, at odds with nature (see, e.g., Niemeijer et al., 2012 for a review).

There are also other, even more fundamental, limitations inherent to the "high velocity" friction laboratory experiments. First, the role of fluids in real faults is likely to be crucial (Miller, 2013; Mulargia and Bizzarri, 2014, 2015), but laboratory experiments cannot realistically account for this due to inevitable technical limitations. Second, experiments forcedly disregard the fracture process, which is instead likely to play a crucial role in natural faulting (see, e.g., Bizzarri, 2011). Third, it is difficult to reproduce a realistic loading history, and the effect of this history on laboratory results has never been analyzed. In practice, there is no evidence that the imposed load function is dynamically consistent with, and that can be taken as representative of, the velocity

* Corresponding author.
E-mail addresses: francesco.mulargia@unibo.it (F. Mulargia), andrea.bizzarri@ingv.it (A. Bizzarri).

http://dx.doi.org/10.1016/j.pepi.2016.06.004
0031-9201/

evolution on natural faults. Finally, the linear consumption (due to either wear and/or melting) in centimeter size laboratory samples is unlikely to be equal to the nonlinear processes occurring in the kilometer size Earth faults.

In conclusion, the results of laboratory experiments should to be regarded as an interesting proxy to natural faulting, but each single piece of evidence should be carefully scrutinized before transferring it to the real world, since the laboratory conditions are still quite far from hypocentral ones. It is therefore hardly surprising that the laboratory slip physics applied to earthquake occurrence may still lead to a number of paradoxes.

The present paper is devoted to analyze how accounting for slip physics not only for what concerns the mechanical terms, and under realistic crustal conditions, may remove such paradoxes. At the end, we also propose a paradox free physical model of the preparatory and coseismic phases which is in agreement with all available observations.

2. The fault slip paradoxes

Let us now briefly review the *fault paradoxes*, the first one of which concerns the fault geometric orientation with respect to the stress field. Let us consider a general stress configuration in the principal stress axis system, i.e. a stress tensor $\sigma_{ij} = \delta_{ij}\sigma^{I,II,III}$, where the stress eigenvalues in the diagonal follow the usual convention $\sigma^{I} > \sigma^{II} > \sigma^{III}$. Eq. (2) defines the planes in which the effective stress attains its maximum value and where Eq. (1) is satisfied. The maximum of σ^{eff} occurs when the maximum compressive stress is at an angle θ with the fault plane (Anderson, 1905)

$$\theta = \frac{1}{2} arctan\left(\frac{1}{\mu}\right) \tag{3}$$

i.e., the orientation of the most favoured slip plane depends on the value of the coefficient of friction. In particular, at the friction coefficient values measured in the laboratory, which are (e.g., Byerlee, 1990) $\mu \sim 0.6$–0.8, the maximum effective stress orientation is at $\sim 30^{\circ}$ degrees to the maximum compression axis. This is odds with observation and leads to the *fault orientation paradox*. In fact, Eq. (3) can be easily inverted and used to estimate the coefficient of friction directly from the seismic focal mechanism. Experimentally, the normal of the slip plane is found to be at an angle with the axis of maximum compression (Zoback et al., 1987; Iio, 1997) consistent with $\mu \sim 0.2$.

Closely related to the above, there is a second paradox, which is tied to the surprisingly small thermal energy produced by earthquakes. In order to see this, let us introduce a seismic source model, which we will simply take as a plane dislocation over a bidimensional plane surface (Brune, 1968) of linear dimension r, and area A proportional to r^2. The energy balance equation – disregarding the gravitational term since its importance depends on the individual fault mechanism and geometry – will include four terms (see e.g. Kanamori and Heaton, 2000; Mulargia et al., 2004; Bizzarri and Cocco, 2006):

$$\Delta E_E = E_R + E_F + E_T \tag{4}$$

where E_E is the stored elastic energy, E_R the elastically radiated energy, E_F is the fracture energy, and E_T the thermal energy, i.e. the energy which is dissipated into heat due to frictional sliding.

Taking as the basic event the average slip $\bar{s}$ on a given patch, the work done by this slip is

$$\Delta W = \bar{\sigma}\bar{s}A = \Delta E_E \tag{5}$$

where $\bar{\sigma}$ is the average stress during the slip. The radiated energy E_R can be directly estimated from the seismic scalar moment $M_0 = G\bar{s}A$ as (see e.g., Kanamori and Brodsky, 2004)

$$\Delta W_R = \Delta\sigma M_0/2G = E_R \tag{6}$$

where $\Delta\sigma$ is the stress drop and G is the rigidity of the medium surrounding the seismic source. At the same time, the fracture energy corresponds to the breaking of bonds required to create new surfaces (Griffith, 1920). This process releases elastic energy mostly in terms of elastic waves, but – given the microscopic bond size – occurs essentially at high frequency >1 kHz, and it is therefore not comprised in the term E_R. The latter concerns rather the emission in the seismic band $\leqslant 10$ Hz, and is related to the macroscopic dislocation.

Estimates of fracture energy E_F made using the elastic approximation alone, which mostly regard the fault as a whole depicted as a single propagating mode III crack (Kostrov, 1966; Eshelby, 1969; Freund, 1998) must be regarded as speculative. It is preferable to rely directly on experimental fracture energy data relative to sliding experiments with realistic "fault gouge", which show that fracture energy is 3–4 orders of magnitude smaller than the total energy (Yoshioka, 1986). As a consequence, since we are not considering the case of fresh faulting, fracture energy can be disregarded.

In light of the general energy balance equation, we have

$$\Delta W_T = \mu\sigma_N\bar{s}A = E_T \tag{7}$$

Thus, by considering Eqs. (5)–(7)

$$\bar{\sigma} = \frac{\Delta\sigma}{2} + \mu\sigma_N \tag{8}$$

and, assuming that slip is confined to a thin region, the rate of heat per unit area $\dot{Q}$ generated by fault slip (i.e. by frictional heating) can be roughly calculated by using the equation for constant heat ux on a plane in an infinite medium as

$$\dot{Q} = \mu\sigma_N v \tag{9}$$

where v is the slip velocity. An alternative would be to consider the detailed material structure, which is obviously not possible in a general treatment. Hence, the temperature rise ΔT after a slip d at constant velocity v can be approximated as (cf. Sibson, 1973)

$$\Delta T = \frac{\mu\sigma_N}{k}\sqrt{\frac{Kdv}{\pi}} \tag{10}$$

where k is the thermal conductivity and K the thermal diffusivity.

Note that taking in Eq. (10) the friction coefficient μ equal to its static value, as we do, is consistent with (a) a slow slip velocity $v \ll v_s$, where v_s is the shear wave velocity and (b) a disregardable cohesion $\sigma^R \sim 0$. Based on laboratory evidence, reasonable values of the parameters involved are $K = 10^{-6}$ m^2/s, $k = 1$ J/(s m °C), yielding temperature increases >1000 °C for velocities and displacements typical of seismic events, since sliding is experimentally concentrated in a zone of 1 cm or less (Kanamori and Heaton, 2000). The paradox lies in the fact that this should induce extensive melting, but the presence of melting products like pseudotachylites is experimentally very rare in real faults. Note also that, on the contrary, pseudotachylites are quite copiously generated in all laboratory friction experiments (cf. Niemeijer et al., 2012, and references therein), underlining the crucial difference between laboratory and real faults that we have discussed above. Such a discrepancy is further confirmed by heat flow measurements along the San Andreas and other faults, which yield a heat production at least five times smaller than expected (Brune et al., 1969; Lachenbruch and Sass, 1980). This constitutes the *fault heat flow paradox*, and calls for some mechanism capable of substantially reducing friction.

In the literature, dynamical mechanisms have been proposed to explain the scarcity of melting products, like thermal pressurization of pore fluids, flash heating of micro-asperity contacts and mechanical lubrication (see Sections 8.3, 8.4 and 8.6 of Bizzarri, 2014 and references cited therein). These processes predict a

significant, often dramatic, decrease of the dynamic frictional resistance, which causes a nearly complete stress drop and, intuitively, a significant decrease in frictional heating (cf. Eq. (9)). However, the same dynamic models of seismic rupture show that the reduction of the frictional resistance leads also to an increase in sliding speed, which in turn raises the temperature (cf. again Eq. (9)). As a net result, all the dynamical mechanisms invoked to solve the heat flux paradox appear incapable to effectively avoid melting.

Finally, note that melting itself might reduce friction, but it should occur much more extensively than it is observed in exhumed faults (cf. Sibson, 1992; Magloughlin and Spray, 1992). Moreover, it must be emphasized that all the above-mentioned physical processes would not alter the *static* friction, which is – on the contrary – the key element of the present study, and therefore are totally incapable of explaining the following third paradox.

The latter consist in the following: the change in seismicity following major earthquakes near the San Andreas fault calls for similarly small values of μ, i.e. $\mu = 0.1 \simeq 0.3$ (Reasenberg and Simpson, 1992), and stress inversion applied to near-surface geological faults relative to microearthquakes in eastern Taiwan consistently give $\mu \leqslant 0.2$ (Reches, 1987, Fig. 6b). This evidence stands for a third paradox, closely tied to the other two and possibly at their very basis, which we may simply call the *friction coefficient paradox*.

3. The multi stage earthquake process

Given the long time scale of geologic phenomena with respect to earthquake occurrence, we may assume that the stress field coincides with the regional tectonic stress field, i.e. that Eqs. (1) and (2) relate to very similar stress matrices for all earthquake recurrences on a given fault.

The initial slip at high friction constitutes the first stage of the slow ignition model that we propose in the present paper. This will occur on planes with orientation relative to $\mu \sim 0.7$, i.e., at $\sim 30°$ to the maximum compression axis (see Eqs. (1) and (2)) comprised within the pre-existent fault volume (see Fig. 1). Such "en echelon" orientation with respect to the fault is compatible with Riedel cracks (e.g., Tchalenko, 1970) and these initial fractures can possibly be seen as coincident with them. In agreement with laboratory observations, we assume that slip occurs slowly, with $v \leqslant 1$ cm/s, with a radiated elastic energy which is a fraction $\leqslant 10^{-2}$ of the thermal energy (e.g. Lockner and Okubo, 1983), so that $\Delta W \simeq \Delta W_T$. In other words, in this first stage – *stage I* – virtually all the work done by the slip is transformed into heat according to Eq. (9). The spatial and time scales of this first stage will be inferred in the following.

This high friction slip determines a temperature increase of the matter surrounding the slip plane equal to (cf. Mulargia et al., 2004; Bizzarri and Cocco, 2006)

$$\Delta W_T = \Delta Q = CAw\rho \sim Cr^2 w\rho \tag{11}$$

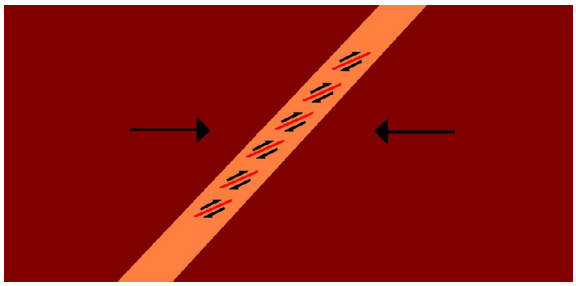

Fig. 1. The stress concentrator patches inside the fault volume optimally oriented with slip at a high static friction of $\mu \sim 0.7$. This slip constitutes stage I.

where C is the specific heat per unit volume, w the width of the *thermal zone*, i.e. of the volume surrounding the slip plane and ρ is the density. The width w over which heat is propagated by thermal diffusion is

$$w(t) \simeq 2\sqrt{Kt} \tag{12}$$

which means that after 10 s from the starting of the slip, the heated front will have propagated in the surrounding volume at a width w of the order of 1 cm.

The temperature increase in this thermal zone will almost immediately induce fluid pressurization and, since permeability in fault gouge is less than 10^{-18} m^{-2} – a virtually impermeable condition (Morrow et al., 1981) – fluid pressure is easily raised from hydrostatic to lithostatic (see Fig. 2). This slip rate required for such an increase can be very slow, since temperature increases of the order of 100°, sufficient to grant pore fluid pressurization at lithostatic level, are attained at velocities of just 0.1 cm/s and displacements of 1 cm. Hence, time scale of the slip and of the thermalization and pressure increase is of the order of 10–100 s, while the related spatial scale is of the order of 1–10 cm.

Heat propagation makes the thermal zone grow larger, and – simultaneously – also cool. The conduction time constant λ is

$$\lambda = w/4K \tag{13}$$

rules the decay of temperature as a function of time t. For our values λ will be of the order of 30 s, which means that the temperature decay will be (cf. Lachenbruch, 1980)

$$T(t) \propto \sqrt{\frac{\lambda}{\pi t}} \tag{14}$$

i.e., once reached the values that guarantee pore fluid pressurization at the lithostatic level, the temperature – and therefore the pressure – will remain high for several tens of seconds. This pressurization constitutes *stage II* (see Fig. 3) and determines a local increase in pore pressure by Δp, thus increasing the effective stress σ^{eff} in neighborhood of the slip patches and countering the decrease in deviatoric stress due to slip. The process continues as long as σ^{eff} is sufficient to overcome cohesion according to Eq. (1). Experimental confirmations of this effect do exist for friction slip on fluid saturated rocks (e.g., Ghabezloo and Sulem, 2009).

The pressurization of fluids around the slip patches radically changes the balance of Eqs. (1) and (2) within the fault volume.

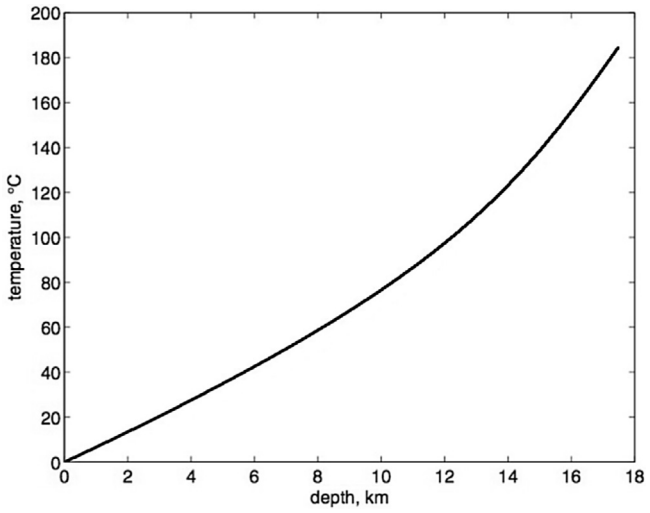

Fig. 2. The temperature increase required to raise the fluid pressure from hydrostatic lithostatic versus depth (redrawn from Burnham et al., 1969).

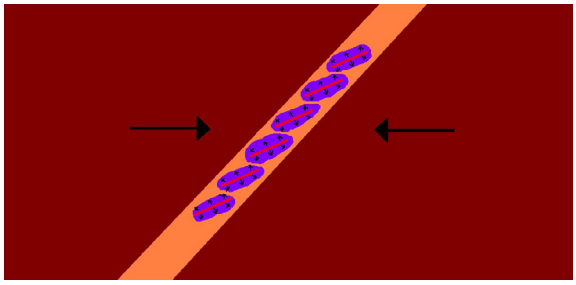

Fig. 3. The pressurization due to the temperature increase produced by the high friction slip. The temperature – and consequently the pressure – increase in the region with width w around the slip patch (see Eq. 11). This constitutes stage II.

The size of the region interested by fluid pressurization increases with time according to Eq. (12). In fact, according to Eq. (14), a temperature increase of 500 °C attained at the slip plane will induce a temperature increase of more than 100 °C after 200 s on a volume of width ∼6 cm surrounding it. If fluids were not present, this could activate dynamic weakening mechanisms. On the contrary, in the real case fluids are indeed present, and this will determine a coalescence of the pressurized regions near the en echelon planes in the fault volume (see Fig. 4). This coalescence constitutes *stage III*, which also involves centimeter size domains, just as the other previous stages. Given the above parameter range, the time and spatial scales of coalescence are of the order of 100–1000 s and 10–100 cm, and concern slips of the order of 1 cm. It is important to remark that we do not rule out melting, but limit its occurrence to local domains and modest amounts, since as soon as heat reaches the fluids it pressurizes them, decreasing friction and thus quenching any further melting.

Consider now the situation: the pre-existent fault volume represents a region of the crust optimally oriented with respect to the regional stress with pore fluids at near lithostatic pressure. In this volume, Eqs. (1) and (2) still apply but, if we keep the initial value of fluid pressure p_0 (which still acts outside the pressurized volume), this will appear as a lower value μ_{press} of the friction coefficient μ

$$\mu_{press} = \mu_0 \frac{\sigma_N - p_0}{\sigma_N - p_{press}} \tag{15}$$

where the "0" and the "*press*" subscripts refer respectively to the non-pressurized state at the beginning of the process and to the pressurized state of stage III. We must still call the latter coefficient "static" since at all stages up to III it relates to a state prior to the seismically radiating fast slip, which is the only one conventionally termed "dynamic".

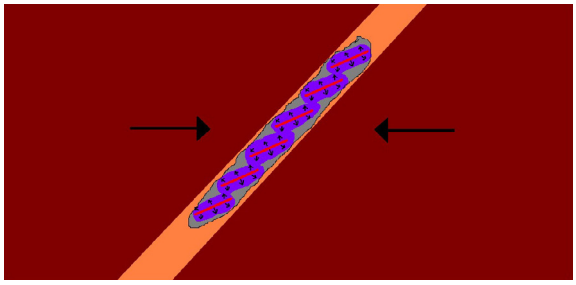

Fig. 4. Heat propagation to larger widths w around the individual slip patches (cf. Eq. 12) leads the locally pressurized zones to coalesce into a connected pressurized volume oriented as the pre-existent fault, which is now ready to slip with an equivalent low friction coefficient (cf. Eq. 15). This constitutes stage III, preparing the system for the low friction fast macroscopic dislocation of stage IV.

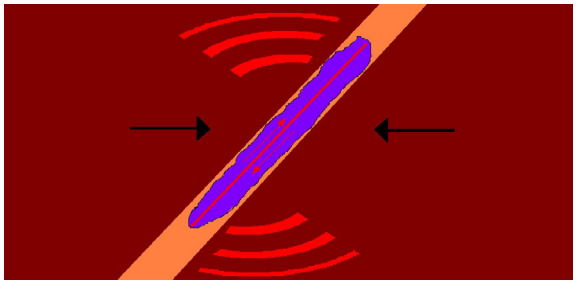

Fig. 5. The low friction elastically radiating slip which constitutes stage IV. During this slip, the friction coefficient can be dynamically reduced to values smaller than the initial 0.2. The rupture extends within the band up to distances from the patch which depend on the correlation length of the stress and fault mechanical structure, i.e., as long as the Tresca–Von Mises condition, Eqs. 1 and 2, is dynamically satisfied (with the dynamic value of the friction coefficient μ in Eq. 2).

As soon as stage III is completed, Eqs. (1) and (2) are simultaneously satisfied and fast, low friction slip can start, releasing most shear energy through seismic radiation, i.e. $E_E \sim E_R$. During this slip, the friction coefficient can be dynamically reduced to even smaller values than the initial one, thus releasing virtually all deviatoric stress. This constitutes *stage IV*, which coincides with the standard dislocation dynamic model of earthquakes (see Fig. 5). The main slip propagates along the strike according to the correlation length of the stress and of the fault mechanical structure, i.e., as long as the Tresca–Von Mises condition, Eq. (1), is dynamically satisfied. This is in agreement with previous dynamic models of earthquake rupture, which describe the dynamic weakening of the fault traction and the propagation of the rupture on the fault even up to large distances from the nucleation patch. Note that slip in stage IV starts at an angle ∼40° to maximum compression, compatible with $\mu \simeq \mu_{press} \sim 0.2$ due to fluid thermal pressurization (see Eq. (15)), and bends further towards 45° in response to the dynamic decrease of μ, but such bending cannot be a stable attractor since fault orientation remains compatible with $\mu \sim 0.2$. A complete treatment of the latter would require to analyze in detail the dynamics of stage IV, which is a highly nonlinear problem beyond the scope of the present work.

4. Discussion and conclusions

The initial slip of stage I needs high stress levels to be initiated. In fact, even if the cohesion energy σ^R in Eq. (1) is $\sigma^R \sim 0$ (cf. Hoek, 1990) and can therefore be disregarded, rewriting Eq. (2) in the principal axes system, with the largest and smallest stress eigenvalues σ^I, σ^{III} written as $\sigma^I = \Delta\sigma^{III}$, with $\Delta \geqslant 1$ gives

$$\frac{\sigma^{eff}}{\sigma^{III}} = \Delta[1 - \mu(1 - cos2\theta)] - \mu\left(1 + cos2\theta - \frac{2p_{fluid}}{\sigma^{III}}\right) - 1 \tag{16}$$

This equation summarizes the dependence of σ^{eff} on applied stress, fluid pressure and friction coefficient, as illustrated in Fig. 6. It is immediate to see that at usual laboratory conditions, i.e., at static friction values $\mu \sim 0.7$ and hydrostatic fluid pressure, σ^{eff} is > 0 – and the slip process can initiate – only when $\sigma^I > 15\sigma^{III}$. Fluid pressures higher than hydrostatic require lower deviatoric stresses, but fluid pressures equal to 75% of the lithostatic still require $\sigma^I > 6\sigma^{III}$ values, while even fluid pressures equal to 90% of the lithostatic require $\sigma^I > 3\sigma^{III}$ values.

Given the in situ stress measurements and the low and constant stress drop values (cf. Mulargia and Bizzarri, 2014, 2015 and references therein), such high deviatoric stresses can only be realized locally by the stress concentration of preexistent cracks. In other words, the slip process can only start at stress concentrators which

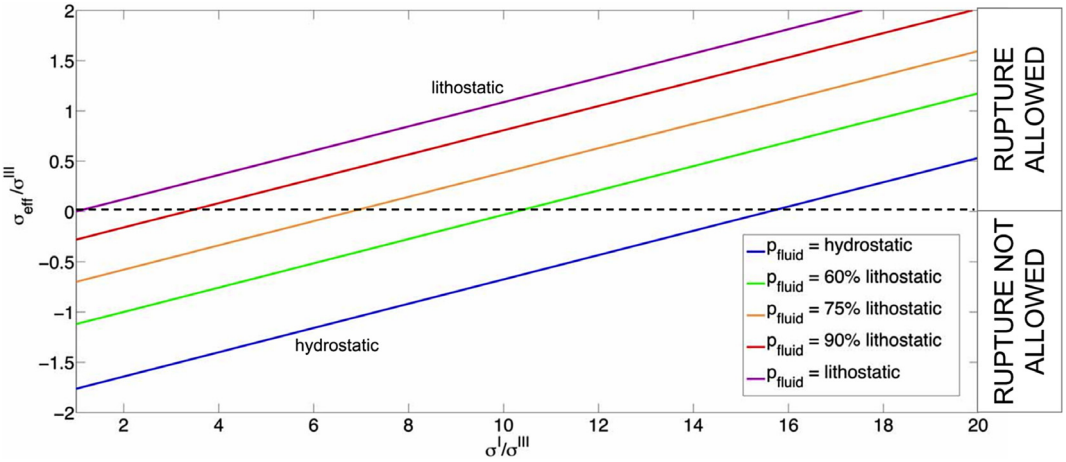

Fig. 6. The Tresca–Von Mises static equation 16 rewritten to give the maximum effective stress σ^{eff}, normalized to the smallest stress eigenvector σ^{III}, as a function of the ratio between the largest and the smallest stress eigenvalues $\Delta = \sigma^{I}/\sigma^{III}$. Different fluid pressure values are considered ranging from hydrostatic to lithostatic. The maximum effective stress value refers to the slip plane oriented according to Eq. 3, with $\mu = 0.7$. The region with $\sigma^{eff}/\sigma^{III} > 0$ represents the domain in which the Tresca–Von Mises condition, Eqs. 1 and 2, is satisfied.

locally increase the deviatoric stress by $\sim$ one order of magnitude, allowing locally the high friction slip of stage I at $\mu = 0.7$. It is the latter slip that, in stage II, induces strong local temperature increases which, in turn, pressurize the surrounding pore fluids.

This initial local slip will be very slow and "silent", i.e. creep-like (cf. the experimental findings of Guglielmi et al., 2015 and those of Witze, 2015), since temperature increases of the order of 10^2 °C, sufficient to grant pore fluid pressurization, are attained for velocities of 0.1 cm/s and displacements of 1 cm, which are well below the limit for elastic radiation (see e.g., Rubin and Ampuero, 2005; Bizzarri and Spudich, 2008).

The heat front around each slip patch propagates, expanding the locally pressurized regions up to the point that the ones coalesce. This induces an equivalent static coefficient of friction $\mu \ll 0.7$ in a volume oriented as the pre-existent fault, i.e. compatible with a static coefficient of friction $\mu \sim 0.2$, as it is routinely observed. To summarize, the fast slip radiating process starts only when the three slow ignition stages of I – high friction slip, II – thermal pressurization, III – heat propagation and coalescence of the thermally pressurized zones – have been completed, which requires times of the order of 100–1000 s and spatial domains (i.e., *slipping patches*) of 10–100 cm. The size of the radiating event is given by the correlation length of the slipping patches. If this is small, and slipping patches are sparse, the sequence may abort before reaching the coalescence stage III, no radiation will be observed, but just localized creep. Otherwise, stage IV will occur, with a dynamic rupture propagation. Both the prolific stage I–stage IV and the aborted stage I–stage II sequences have been apparently observed under fluid injection using fluid pressure values typical of oil industry at an underground laboratory in southeastern France (Witze, 2015). Note that each process will start the stage I–stage IV sequence from the beginning, since the fast dynamic slip of stage IV will destroy most signs of the previous ones. Geologic remnants of stages I–III are likely to be observed only in aborted sequences.

It is interesting to emphasize that in the framework of the present model, stage IV – which is responsible for seismic wave excitation and seismic radiation, and which deals with an extended fault model (rather than a single or coalescent cracks as in previous stages) and coincides with the subject of dynamic models of faulting – starts with a non vanishing sliding speed. In the model proposed in the present paper, the nucleation process (i.e. the preparatory stages leading to dynamic instability in a finite fault zone) is accounted for in stages I–III.

The triggering of a fast radiating slip by fluid pressure waves or by dynamic or static external stresses may act at all stages, but it is only at stage I that it can be crucially effective, when even very small stresses may trigger the process in a system which is close to the critical state (cf. Mulargia and Bizzarri, 2014, 2015).

Our proposed physical model considers the total energy balance of the system, rather than just the mechanical terms, as it usually happens in the seismological approach. In this picture, the thermal balance is found to play a key role together with fluid flow, which acts as the basic trigger for the whole process, reaching the faults through high permeability material discontinuities, i.e., joints and fractures. Once at the boundary of the system, flow occurs slowly through pores into the low permeability gouge and the process starts according to Eq. (1), as is experimentally supported by the permeability parameters measured in reservoir induced earthquakes (Talwani et al., 2007).

The first three stages of the process involve small spatial domains of less than a meter size, but the dimension of the radiating event is given by the extent of the spatial domain in which stages I–III occur, i.e. by the correlation length of the slipping patches. However, the correlation length is ruled by the fine structure of the system at the slip patch size at sub-meter lengths, which is practically knowable only in statistical sense. Hence, the final dimension of the event is already set at the beginning of the process, but it is unrealistic to measure it because it is not broadcasted before the process ends the fast propagation of stage IV. In other words, the system knows beforehand how big will the earthquake be, but won't tell it because the first three stages are seismically asymptomatic and because they involve single volumes which are many orders of magnitude (up to 10) smaller than those which the earthquake will finally involve.

Hence, our first three stages cannot represent the slow initial moment release of the cascade nucleation model (Ellsworth and Beroza, 1995), which could rather coincide with the dynamic decrease of the friction coefficient, thus splitting stage IV into further substages. At odds with this model – in which an earthquake occurs as the net result of the sequential chain triggering of multiple small events – the staged ignition model we have developed here is in the same perspective of pre-slip models (e.g., Okubo, 1989), in which failure starts aseismically with a slow sliding over limited regions of the fault zone, and gradually expands to become unstable when it reaches a critical size. In our model, this critical

size is the correlation length sufficient to start fast slip with radiation in the seismic band.

Acknowledgements

The authors are indebted to an anonymous referee, whose comments substantially improved the paper.

References

Anderson, E.M., 1905. The dynamics of faulting. Trans. Edinburgh Geol. Soc. 8, 387–402.
Bizzarri, A., 2011. On the deterministic description of earthquakes. Rev. Geophys. 49 (RG3002). http://dx.doi.org/10.1029/2011RG000356.
Bizzarri, A., 2014. The mechanics of seismic faulting: recent advances and open issues. Riv. Nuovo Cimento 37 (4), 181–271. http://dx.doi.org/10.1393/ncr/i2014-10099-0.
Bizzarri, A., Cocco, M., 2006. A thermal pressurization model for the spontaneous dynamic rupture propagation on a three-dimensional fault: 1. Methodological approach. J. Geophys. Res. 111, B05303. http://dx.doi.org/10.1029/2005JB003862.
Bizzarri, A., Spudich, P., 2008. Effects of supershear rupture speed on the high-frequency content of S waves investigated using spontaneous dynamic rupture models and isochrone theory. J. Geophys. Res. 113, B05304. http://dx.doi.org/10.1029/2007JB005146.
Brune, J.N., 1968. Seismic moment, seismicity, and rate of slip along major fault zones. J. Geophys. Res. 73, 777–784.
Brune, J.N., Henyey, T.L., Roy, R.F., 1969. Heat flow, stress and rate of slip along the San Andreas Fault, California. J. Geophys. Res. 74, 3821–3827.
Burnham, C.W., Holloway, J.R., Davis, N.F., 1969. Thermodynamic properties of water to 1000 C and 10,000 bars. Geol. Soc. Am. Spec. Paper, Paper 132.
Byerlee, J.D., 1990. Friction, overpressure and fault normal compression. Geophys. Res. Lett. 17, 2109–2122.
Di Toro, G. et al., 2010. From field geology to earthquake simulation: a new state-of-the-art tool to investigate rock friction during the seismic cycle (SHIVA). Rend. Fis. Acc. Lincei 21, S9504S114. http://dx.doi.org/10.1007/s12210-010-0097-x.
Ellsworth, W.L., Beroza, G.C., 1995. Science 268, 851–855. http://dx.doi.org/10.1126/science.268.5212.851.
Eshelby, J.B., 1969. The elastic field of a crack extending nonuniformly under general anti-plane loading. J. Mech. Phys. Solids 17, 177–199.
Freund, L.B., 1998. Dynamic Fracture Mechanics. Cambridge University Press, New York, 598 p.
Ghabezloo, S., Sulem, J., 2009. Stress dependent thermal pressurization of a fluid-saturated rock. Rock Mech. Rock Eng. 42, 1–24.
Griffith, A.A., 1920. The phenomena of rupture and flow in solids. Phil. Trans. R. Soc. Lond A. A221, 163–198.
Guglielmi, Y., Cappa, F., Avouac, J.P., Henry, P., Elsworth, D., 2015. Seismicity triggered by fluid injection induced aseismic slip. Science 348, 1124–1226. http://dx.doi.org/10.1126/science.476.
Hoek, E., 1990. Estimating Mohr–Coulomb friction and cohesion values from the Hoek–Brown failure criterion. Int. J. Rock Mech. Min. Sci. & Geomech. Abstr. 27, 227–229.
Iio, Y., 1997. Frictional coefficient on faults in a seismogenicregion inferred from earthquake mechanism solutions. J. Geophys. Res. 102, 5403–5412.
Kanamori, H., Heaton, T.H., 2000. Microscopic and macroscopic physics of earthquakes. In: Rundle, J.B., Turcotte, D.L., Klein, W. (Eds.), Geocomplexity and the Physics of Earthquakes. AGU Publ., Washington, pp. 147–194.
Kanamori, H., Brodsky, E.E., 2004. The physics of earthquakes. Rep. Prog. Phys. 67, 1429–1496.
Kostrov, B.V., 1966. Unsteady propagation of longitudinal shear cracks. J. Appl. Math. Mech. (transl. P.M.M.) 30, 1241–1248.
Lachenbruch, A.H., 1980. Frictional heating, fluid pressure, and the resistance to fault motion. J. Geophys. Res. 85, 6097–6122.
Lachenbruch, A.H., Sass, J.H., 1980. Heat flow and energetics of the San Andreas fault zone: Magnitude of deviatoric stresses in the Earth's crust and uppermost mantle. J. Geophys. Res. 85, 6185–6222.
Lockner, D.A., Okubo, P.G., 1983. Measurements of frictional heating in granite. J. Geophys. Res. 88, 4313–4320.
Magloughlin, J.F., Spray, J.G., 1992. Frictional melting processes and products in geological materials: introduction and discussion. Tectonophysics 204, 1976.
Miller, S.A., 2013. The role of fluids in tectonic and earthquake processes. Adv. Geophys. 54, 1–46. http://dx.doi.org/10.1016/B978-0-12-380940-7.00001-9.
Morrow, C.A., Shi, L.Q., Byerlee, J.D., 1981. Permeability and strength of San Andreas fault gouge under high pressure. Geophys. Res. Lett. 8, 325–328.
Mulargia, F., Castellaro, S., Ciccotti, M., 2004. Earthquakes as three stage processes. Geophys. J. Int. 158, 98–108.
Mulargia, F., Bizzarri, A., 2014. Anthropogenic triggering of large earthquakes. Nature Sci. Rep. 4 (6100), 1–7. http://dx.doi.org/10.1038/srep06100.
Mulargia, F., Bizzarri, A., 2015. Fluid pressure waves trigger earthquakes. Geophys. J. Int. 200 (3), 1281–1285. http://dx.doi.org/10.1093/gji/ggu469.
Niemeijer, A., Di Toro, G., Griffith, W.A., Bistacchi, A., Smith, S.A.F., Nielsen, S., 2012. Inferring earthquake physics and chemistry using an integrated field and laboratory approach. J. Struct. Geol. 39, 24–36.
Ohnaka, M., 2013. The Physics of Rock Failure and Earthquakes. Cambridge Univ. Press.
Okubo, P.G., 1989. Dynamic rupture modeling with laboratory-derived constitutive relations. J. Geophys. Res. 94, 12321–12335.
Reasenberg, P.A., Simpson, R.W., 1992. Response of regional seismicity to the static stress change produced by the Loma Prieta earthquake. Science 255, 1687–1690.
Reches, Z., 1987. Determination of the tectonic stress tensor from slip along faults that obey the Coulomb yield condition. Tectonics 6, 849–861.
Rubin, A.M., Ampuero, J.-P., 2005. Earthquake nucleation on (aging) rate-and-state faults. J. Geophys. Res. 110, B11312. http://dx.doi.org/10.1029/2005JB 003686.
Sibson, R.H., 1973. Interactions between temperature and pore fluid pressure during earthquake faulting – a mechanism for partial or total stress relief. Nature 243, 66.
Sibson, R.H., 1992. Power dissipation and stress levels during seismic faulting. J. Geophys. Res. 85, 6239–6247.
Sone, H., Shimamoto, T., 2009. Frictional resistance of faults during accelerating and decelerating earthquake slip. Nature Geosci. 2. http://dx.doi.org/10.1038/NGEO637.
Talwani, P., Chen, L., Gahalaut, K., 2007. Seismogenic permeability, k_s. J. Geophys. Res. 112, B07309. http://dx.doi.org/10.1029/2006JB004665.
Tchalenko, J.S., 1970. Similarities between shear zones of different magnitudes. Bull. Geol. Soc. Am. 81, 1625–1640.
Terzaghi, K., Peck, R.B., Mesri, G., 1996. Soil Mechanics in Engineering Practice, third ed. John Wiley, Hoboken, N.J., 592 p.
Witze, A., 2015. Fluid injection causes ground to creep before quakes. Nature 79, F641. http://dx.doi.org/10.1038/nature.2015.17727.
Yoshioka, N., 1986. Fracture energy and the variation of gouge and surface roughness during frictional sliding of rocks. J. Phys. Earth 34, 335–355.
Zoback, M.D. et al., 1987. New evidence on the state of stress of the San Andreas fault system. Science 238, 1105–1111.